Nucleus accumbens feedforward inhibition circuit promotes cocaine self-administration

Jun Yu[a], Yijin Yan[a], King-Lun Li[a], Yao Wang[b], Yanhua H. Huang[b], Nathaniel N. Urban[c], Eric J. Nestler[d,e], Oliver M. Schlüter[a,f], and Yan Dong[a,b,1]

[a]Department of Neuroscience, University of Pittsburgh, Pittsburgh, PA 15260; [b]Department of Psychiatry, University of Pittsburgh, Pittsburgh, PA 15260; [c]Department of Neurobiology, University of Pittsburgh, Pittsburgh, PA 15260; [d]Fishberg Department of Neuroscience, Icahn School of Medicine at Mount Sinai, New York, NY 10029; [e]Friedman Brain Institute, Icahn School of Medicine at Mount Sinai, New York, NY 10029; and [f]Department of Psychiatry and Psychotherapy, University Medical Center, 37075 Göttingen, Germany

Edited by Susan G. Amara, National Institutes of Health, Bethesda, MD, and approved August 29, 2017 (received for review May 11, 2017)

The basolateral amygdala (BLA) sends excitatory projections to the nucleus accumbens (NAc) and regulates motivated behaviors partially by activating NAc medium spiny neurons (MSNs). Here, we characterized a feedforward inhibition circuit, through which BLA-evoked activation of NAc shell (NAcSh) MSNs was fine-tuned by GABAergic monosynaptic innervation from adjacent fast-spiking interneurons (FSIs). Specifically, BLA-to-NAcSh projections predominantly innervated NAcSh FSIs compared with MSNs and triggered action potentials in FSIs preceding BLA-mediated activation of MSNs. Due to these anatomical and temporal properties, activation of the BLA-to-NAcSh projection resulted in a rapid FSI-mediated inhibition of MSNs, timing-contingently dictating BLA-evoked activation of MSNs. Cocaine self-administration selectively and persistently upregulated the presynaptic release probability of BLA-to-FSI synapses, entailing enhanced FSI-mediated feedforward inhibition of MSNs upon BLA activation. Experimentally enhancing the BLA-to-FSI transmission in vivo expedited the acquisition of cocaine self-administration. These results reveal a previously unidentified role of an FSI-embedded circuit in regulating NAc-based drug seeking and taking.

fast-spiking interneuron | medium spiny neuron | basolateral amygdala | synaptic plasticity | cocaine addiction

The nucleus accumbens (NAc) regulates motivated behaviors, a process that requires fine-tuned functional output of medium spiny principal neurons (MSNs) (1, 2). Lacking intrinsic pace-making mechanisms, activation of NAc MSNs is primarily driven by long-distance excitatory inputs (3), among which the projection from the basolateral amygdala (BLA) has been critically implicated in cue-induced motivated behaviors under physiological and pathophysiological conditions (4, 5). In vivo recording reveals that stimulation of the BLA monosynaptically activates NAc MSNs but that the activation is not linear, often with unique temporal patterns (3, 6, 7). In behavioral models of reward seeking, exposure to cues previously associated with the reward activates BLA neurons, but NAc MSNs are not homogeneously activated (8, 9). These circuit and behavioral results suggest that the responsiveness of NAc MSNs to cue-induced BLA activation is finely gated by timing-contingent inhibitory mechanisms.

A potential candidate providing such timing-contingent inhibition is the fast-spiking interneuron (FSI). Although contributing <1% of the NAc neuronal population, FSIs extensively innervate MSNs with an inhibitory network covering the entire striatum (10). In the striatum and other regions, FSIs are activated by the same excitatory inputs that activate principal neurons to provide timing-contingent feedforward inhibition (10, 11). While these properties position FSIs as an effective regulator of the output circuits in general, the cellular and circuit properties of NAc FSIs and their roles in motivated behaviors remain largely unexplored.

Targeting this knowledge gap, our current study uses a knock-in mouse line, in which endocannabinoid receptor 1 (CB1)-expressing neurons are genetically labeled with tdTomato (12). Within the NAc shell (NAcSh), all CB1-expressing neurons are exclusively FSIs, with biophysical and connectivity properties indistinguishable from parvalbumin (PV)-expressing FSIs (12, 13). Our results show that NAcSh FSIs receive a much higher intensity of BLA-to-NAc excitatory inputs than MSNs. Upon optogenetic activation of the BLA-to-NAc projection that evoked excitatory postsynaptic potentials in both FSIs and MSNs, FSIs were activated first to fire action potentials, with the resulting feedforward inhibition blunting the firing of MSNs. Cocaine self-administration did not affect the FSI-to-MSN connectivity in the NAcSh but persistently potentiated the BLA-to-FSI transmission. Mimicking this effect of cocaine by optogenetically inducing long-term potentiation (LTP) at NAcSh BLA-to-FSI synapses in vivo expedited the acquisition of cocaine self-administration. These results demonstrate a previously unidentified role of an FSI-mediated NAc feedforward circuit in cue-induced cocaine seeking and taking.

Results

Excitatory Innervation Exerts a Stronger Effect on FSIs than MSNs. In all experiments, the recording bath was antagonist-free unless specified. In brain slices prepared from CB1-tdTomato knock-in mice, CB1-expressing neurons in the NAcSh were exclusively FSIs (Fig. 1 *A* and *B*), with very different membrane properties compared with principal MSNs, including a relatively depolarized resting membrane potential, high membrane resistance, and short delay of action potential initiation (12). All of these membrane properties may contribute to the fast response of NAcSh FSIs (discussed below). Compared with NAcSh MSNs, CB1-expressing FSIs (abbreviated as FSIs hereafter) exhibited much higher frequencies and larger amplitudes of miniature (m) excitatory postsynaptic currents (EPSCs), with faster activation

Significance

The nucleus accumbens (NAc) regulates cue-induced motivated behaviors, a process that requires fine-tuned functional output of medium spiny principal neurons (MSNs). Our present study reveals that, although contributing <1% of the NAc shell (NAcSh) neuronal population, fast-spiking interneurons (FSIs) form an inhibitory feedforward circuit to dictate the functional output of NAc MSNs. Cocaine self-administration, a rodent model mimicking human cocaine seeking and taking, persistently potentiates the driving force to this FSI-embedded feedforward circuit. Functionally mimicking this effect of cocaine in vivo expedites the acquisition of cocaine self-administration. These results demonstrate a previously unidentified role of an FSI-mediated NAcSh feedforward circuit in cue-induced cocaine seeking and taking.

Author contributions: J.Y., Y.Y., K.-L.L., Y.W., Y.H.H., N.N.U., E.J.N., O.M.S., and Y.D. designed research; J.Y., Y.Y., K.-L.L., and Y.W. performed research; J.Y., Y.Y., K.-L.L., and Y.W. analyzed data; and J.Y., Y.H.H., N.N.U., E.J.N., O.M.S., and Y.D. wrote the paper.

The authors declare no conflict of interest.

This article is a PNAS Direct Submission.

[1]To whom correspondence should be addressed. Email: yandong@pitt.edu.

This article contains supporting information online at www.pnas.org/lookup/suppl/doi:10.1073/pnas.1707822114/-/DCSupplemental.

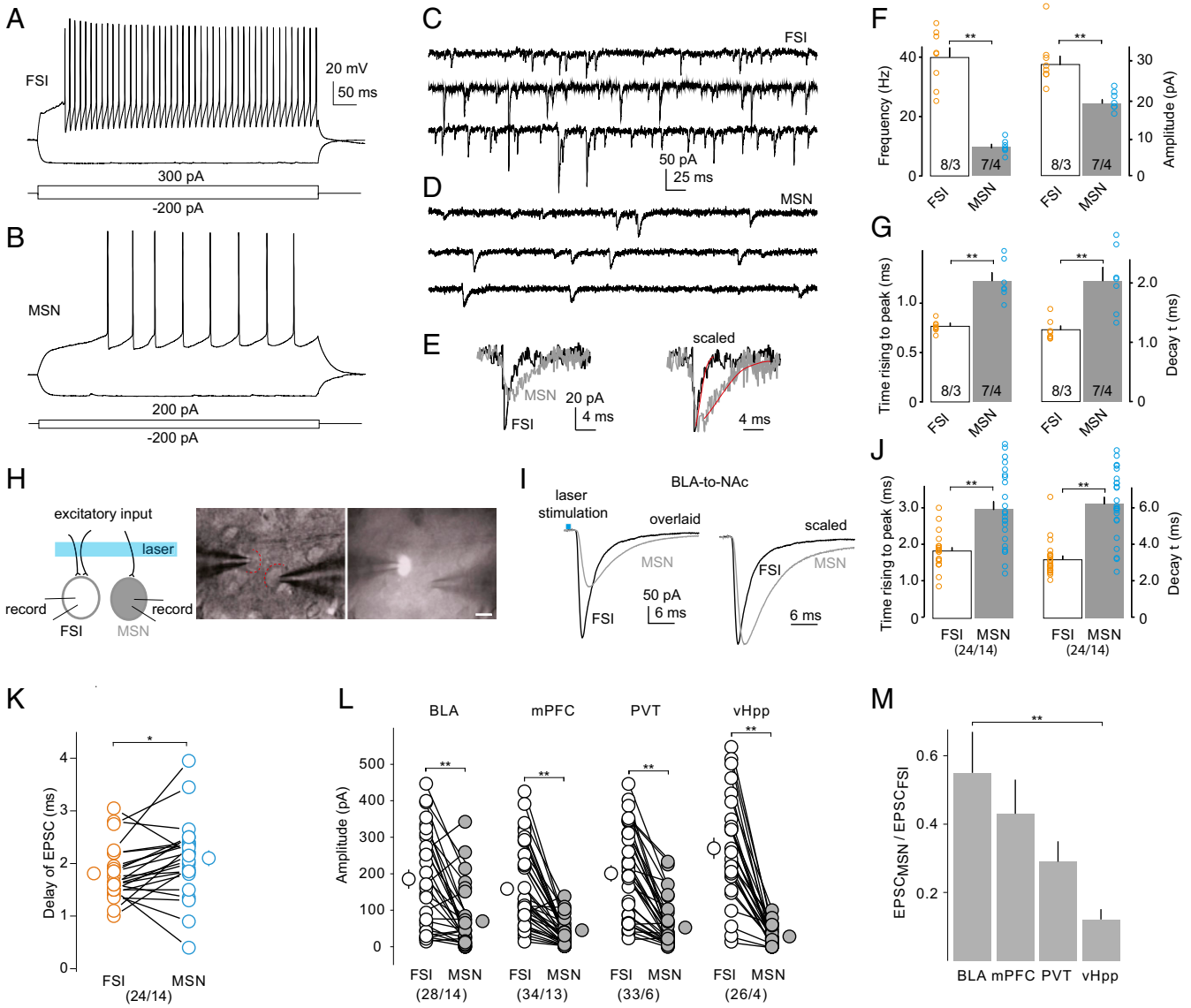

Fig. 1. NAcSh FSIs receive denser excitatory inputs than MSNs. (*A* and *B*) Example traces showing distinct membrane properties between NAcSh FSIs (*A*) and MSNs (*B*). $n > 10$ in each case. (*C*–*G*) Example traces and summarized results showing that compared with NAcSh MSNs, FSIs exhibited higher mEPSC frequencies (in hertz: FSI, 39.8 ± 3.6, $n = 8/3$; MSN, 9.9 ± 1.0, $n = 7/4$; $P = 0.00$, *t* test), larger mEPSC amplitudes (FSI, 29.7 ± 2.4 pA, $n = 8/3$; MSN, 19.5 ± 1.0 pA, $n = 7/4$; $P = 0.00$, *t* test), and faster activation (FSI, 0.76 ± 0.02 ms, $n = 8/3$; MSN, 1.22 ± 0.08 ms, $n = 7/4$; $P = 0.00$, *t* test) and inactivation kinetics of mEPSCs (FSI, 1.20 ± 0.07 ms, $n = 8/3$; MSN, 2.05 ± 0.22 ms, $n = 7/4$; $P = 0.00$, *t* test). (*H*) Diagram and image showing pairwise recording of an NAcSh FSI and an MSN in response to optogenetic stimulation of projection-specific excitatory inputs. (Calibration bar, 20 μm.) (*I*) Example pairwise recording showing that EPSCs were evoked in an FSI and an MSN by the same optogenetic stimulation of the BLA-to-NAc projection. (*J*) Summarized results showing that EPSCs from BLA-to-FSI synapses exhibited faster rising (FSI, 1.8 ± 0.1 ms; MSN, 3.0 ± 0.2 ms; $n = 24/14$; $P = 0.00$, paired *t* test) and decay kinetics (FSI, 3.1 ± 0.2 ms; MSN, 6.2 ± 0.4 ms; $n = 24/14$; $P = 0.00$, paired *t* test) than BLA-to-MSN synapses. (*K*) Summarized results showing that the BLA-to-FSI transmission exhibited shorter synaptic delay than BLA-to-MSN transmission (FSI, 1.8 ± 0.1 ms; MSN, 2.1 ± 0.2 ms; $n = 24/14$; $P = 0.03$, paired *t* test). (*L*) Summarized results of FSI-MSN pairwise recordings showing that BLA-, mPFC-, PVT-, and vHpp-to-NAc projections all evoked EPSCs with larger amplitudes in FSIs than in MSNs. (*M*) Summarized results showing the ratios of the EPSC amplitudes in MSNs to the EPSC amplitudes in pairwise recorded FSIs ($EPSC_{MSN}/EPSC_{FSI}$) at synapses from different projections (BLA, 0.55 ± 0.12, $n = 28/14$; mPFC, 0.43 ± 0.10, $n = 34/13$; PVT, 0.29 ± 0.06, $n = 33/6$; vHpp, 0.12 ± 0.06, $n = 26/4$; $F_{3,117} = 4.389$, $P = 0.006$, one-way ANOVA). *$P < 0.05$, **$P < 0.01$.

and inactivation kinetics (Fig. 1 *C*–*G*). The higher mEPSC frequency suggests a higher presynaptic releasing probability or higher density of synaptic innervation. Excitatory synapses on NAcSh FSIs are highly enriched in calcium-permeable (CP) AMPA receptors (AMPARs) (discussed below), and their high conductance (14) may serve as one of the key postsynaptic mechanisms mediating high mEPSC amplitudes.

To delineate the BLA-to-NAc projection, we bilaterally injected channelrhodopsin 2 (ChR2)-expressing adeno-associated virus 2 (AAV2) into the BLA of anesthetized mice. Approximately 4 wk later, we obtained NAc slices to perform pairwise simultaneous recordings of FSIs and MSNs while activating the BLA-to-NAc projection (Fig. 1*H*). Laser stimulation (at 473 nm) of the same set of BLA-to-NAc fibers resulted in monosynaptic responses in simultaneously recorded FSIs and adjacent MSNs (Fig. 1*I*). The activation and inactivation kinetics of the evoked EPSCs in FSIs were substantially faster than in MSNs, and the delay of the EPSC onset was also shorter in FSIs (Fig. 1 *J* and *K*). The fast activation suggests that FSIs bear excitatory synapses closer to the soma or synapses with faster electrotonic properties compared with MSNs,

while the fast inactivation may be attributable to the fast inactivation kinetics of CP-AMPARs (14), which are highly enriched in FSIs. Such sharp EPSC kinetics allow FSIs to exert fast and precise feedforward inhibition of MSNs. Pairwise comparisons of EPSC amplitudes reveal BLA-to-NAc excitatory inputs produce higher excitation in FSIs than MSNs, and this polarized innervation pattern held true for the projections from the ventromedial prefrontal cortex (mPFC), paraventricular thalamus (PVT), and ventral hippocampus (vHpp) (Fig. 1 *L* and *M*). Collectively, excitatory inputs to the NAcSh exert much greater impact on FSIs than MSNs.

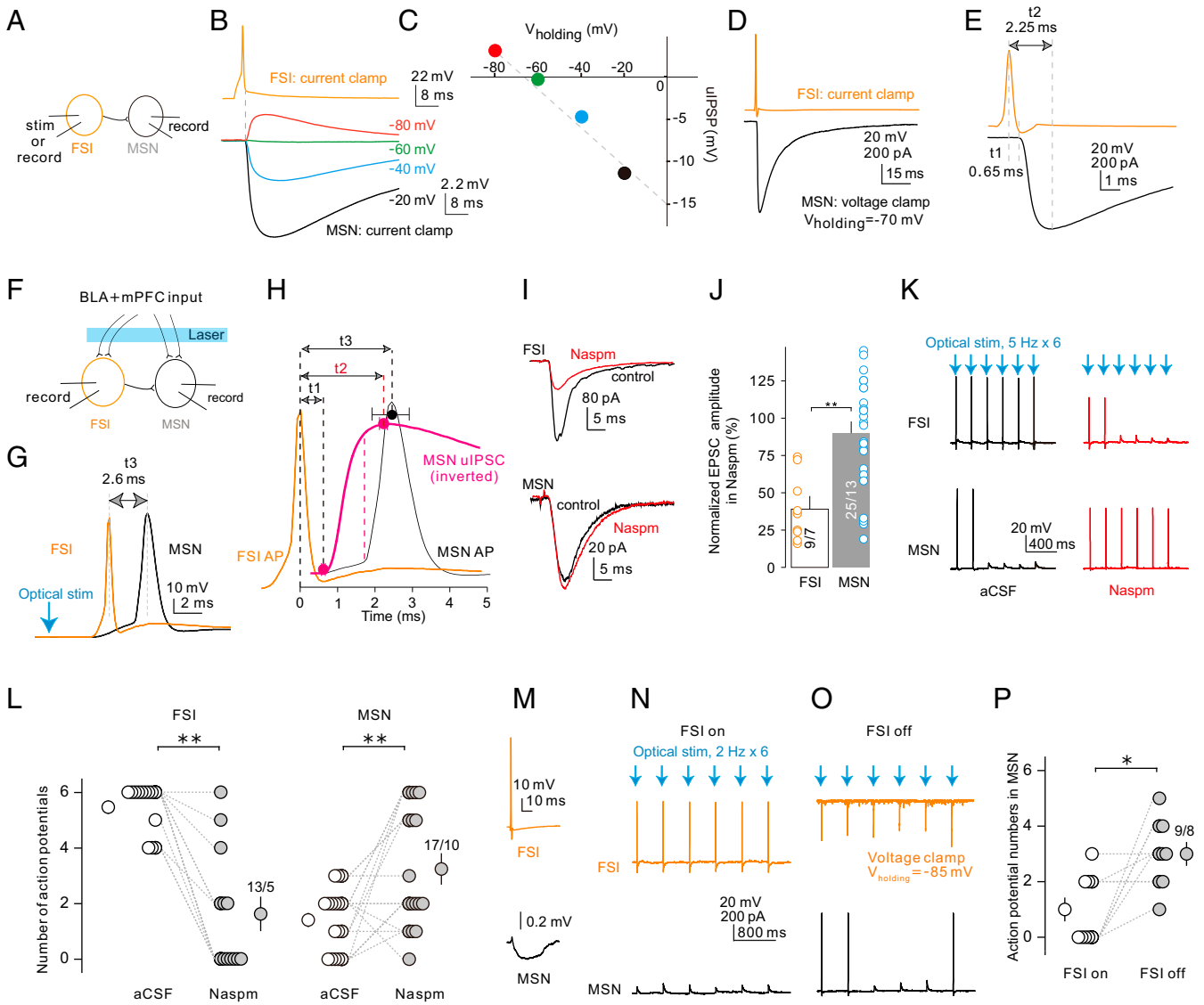

Fig. 2. FSI-mediated feedforward inhibition of NAcSh MSNs. (*A*) Diagram showing a pairwise recording of an FSI and an MSN in the NAcSh. (*B* and *C*) uIPSPs (*B*) and the "V-V" curve (*C*) showing an example paired recording in which stimulation of the FSI evoked monosynaptic uIPSPs in the MSN at different holding potentials, with a reversal potential of ∼−60 mV. (*D* and *E*) An example paired recording showing that an action potential in the FSI evoked an uIPSC in the MSN (*D*), with the time elapsed from the action potential peak to the initiation of uIPSC (t1) of 0.65 ms, and the time from the action potential peak to the uIPSC peak (t2) of 2.25 ms (*E*). (*F*) Diagram showing paired recording of an FSI and an MSN in response to optogenetic stimulation of BLA- and mPFC-to-NAc projections. (*G*) Upon a single optogenetic stimulation of BLA- and mPFC-to-NAc projections, an example pairwise recording showing that action potentials were sequentially evoked in the FSI and MSN with a 2.6-ms delay (t3). (*H*) Summarized results showing the mean t1, t2, and t3 in pairwise recordings in which FSIs innervated MSNs (t1, 0.6 ± 0.1 ms, $n = 17/5$; t2, 2.2 ± 0.1 ms, $n = 17/5$; t3, 2.4 ± 0.5 ms, $n = 7/6$). The FSI-generated uIPSC in MSNs is inverted to manifest its coincidence with the action potential. (*I* and *J*) Example traces (*I*) and summarized results (*J*) showing that application of Naspm preferentially inhibits EPSCs in FSIs, with minimal effects on EPSCs in MSNs in naïve mice (percent amplitude in Naspm: FSI, 39.4 ± 7.8, $n = 9/7$; MSN, 90.0 ± 7.4, $n = 25/13$; $P = 0.00$, *t* test). (*K* and *L*) Example traces (*K*) and summarized results (*L*) showing that preferentially inhibiting excitatory inputs to FSIs by Naspm decreased and increased the likelihood of optogenetically evoked action potential firing in FSIs and MSNs, respectively (number of action potentials: FSI-aCSF, 5.5 ± 0.3, FSI-Naspm, 1.6 ± 0.6, $n = 13/5$, $P = 0.00$, paired *t* test; MSN-aCSF, 1.4 ± 0.3, MSN-Naspm, 3.2 ± 0.5, $n = 17/10$, $P = 0.00$, paired *t* test). (*M*) An example pairwise recording using physiologically relevant internal solutions showing that an action potential firing in the FSI evoked a hyperpolarization of the membrane potential of the MSNs, indicating the FSI–MSN connectivity. Note that the amplitude of the hyperpolarization was small when evoked at the resting membrane potential. (*N* and *O*) Example recordings of the same pair verified in *M* showing that an optogenetic stimulation train (2 Hz × 6 with 1-ms stimulation duration) of the BLA- and mPFC-to-NAc projections evoked action potentials only in the FSI (*N*), but when the FSI was voltage-clamped at −85 mV to prevent action potential firing, the same optogenetic stimulation train evoked action potentials in the MSN (*O*). (*P*) Summarized results showing that preventing action potential firing of a single FSI that innervated the MSN effectively increased the likelihood of action potential firing evoked by optogenetic stimulation of BLA- and mPFC-to-NAc projections (number of action potentials: FSI on, 1.0 ± 0.4; FSI off, 3.0 ± 0.43; $n = 9/8$; $P = 0.02$, paired *t* test). $^*P < 0.05$, $^{**}P < 0.01$.

FSI-Mediated Feedforward Inhibition. NAcSh FSIs exert feedforward inhibition of MSNs through their monosynaptic connections (12, 13). In the pairwise recording setup, we made whole-cell current-clamp recordings of an FSI and an adjacent MSN in the NAcSh (Fig. 2*A*). In this experiment, QX314 (2 mM) was included in the potassium-based electrode solution for MSN recordings to prevent action potential firing at depolarized holding potentials, and AM251 (2 μM) was included in the bath to prevent potential CB1-mediated modulation of synaptic activity. An action potential in the FSI elicited a fast unitary (u) inhibitory postsynaptic potential (IPSP) in its connected MSN at most holding potentials, with the reversal potential of ∼−60 mV (Fig. 2 *B* and *C*). In our experimental conditions, FSI-to-MSN synaptic transmission was detected in 21 out of 42 of the recorded pairs (Fig. S1*E*), with the connectivity rate similar to previous results (13).

We next examined the timing of the FSI-mediated feedforward inhibition. For this set of experiments, we made current-clamp recordings of FSIs and voltage-clamp recordings of MSNs, respectively. We used a high-Cl^-, Cs^+-based electrode solution for MSN recordings such that large inward IPSCs were elicited at −70 mV. In the pairwise recording, a 2-ms current injection evoked an action potential in the FSI, which, in turn, elicited an IPSC in the MSN (Fig. 2*D*). The time elapsed from the peak of the FSI action potential to the onset of the IPSC in the MSN was ∼0.6 ms (t1), and the time elapsed from the peak of the action potential in the FSI to the peak of the IPSC in the MSN was ∼2 ms (t2), consistent with monosynaptic GABAergic transmission (Fig. 2*E*).

With these delays (t1 and t2) of FSI-generated IPSCs, what form of timing contingency does the FSI-mediated feedforward inhibition confer on MSNs upon activation of the same excitatory inputs? To address this, we optogenetically stimulated the BLA- and mPFC-to-NAc projections in NAc slices (Fig. 2*F*). Previous studies reveal that an effective activation of NAc MSNs requires convergent activation of multiple projections, including the BLA and mPFC projections (3). Our pilot results confirmed that under our experimental conditions optogenetic stimulation of either BLA- or mPFC-to-NAc projection alone using physiologically relevant parameters (e.g., stimulation duration ≤1 ms) did not trigger action potential firing in most recorded MSNs (Fig. S2 *A* and *B*), while simultaneous stimulation of BLA- and mPFC-to-NAc projections increased the likelihood of inducing action potentials in MSNs. Upon optogenetic stimulation of BLA- and mPFC-to-NAc projections, the onset of action potentials in FSIs consistently preceded action potentials in MSNs (t3; Fig. 2*G*). Factoring in all these timing parameters after activation of excitatory inputs, in MSNs the peak of the IPSC was coincidental to the peak of the action potential, with the onset (0.6 ± 0.1 ms after FSI action potential peak, $n = 17/5$) of the IPSC ∼1.2 ms preceding the onset (time point at which dV/dt = 10 mV/ms) of the action potential in the MSN (1.8 ± 0.5 ms after FSI action potential peak, $n = 7/6$) (Fig. 2*H*). These circuit properties predict that upon activation of the same excitatory inputs the FSI-mediated feedforward inhibition is initiated before the initiation of the action potential in MSNs, and is therefore capable of compromising even the very first action potential in MSNs upon activation of the same excitatory inputs.

To test this prediction, we first used a pharmacological approach by taking advantage of the fact that excitatory synapses on FSIs and MSNs are enriched in CP-AMPARs and non-CP-AMPARs, respectively (12). As such, optogenetically elicited excitatory inputs to FSIs, but not MSNs, were preferentially inhibited by the CP-AMPAR–selective antagonist Naspm (200 μM) (Fig. 2 *I* and *J*). We applied a six-pulse optogenetic stimulation (5 Hz; pulse duration 1 ms) to the BLA- and mPFC-to-NAc projections, which evoked four to six action potentials in FSIs but many fewer action potentials in MSNs (Fig. 2 *K* and *L*). Application of Naspm decreased action potential firing in FSIs evoked by optogenetic activation of the BLA and mPFC projections but increased action potential firing in MSNs (Fig. 2 *K* and *L*). Note that Naspm also affected action potential amplitudes (Fig. S2 *C* and *D*), suggesting its nonsynaptic effects.

FSIs are sparse in the striatum (10), predicting that the feedforward inhibition of a large number of MSNs can be achieved by a very small number of FSIs. To test this, we made pairwise current-clamp recordings of an NAcSh MSN and an FSI that innervated the MSN (Fig. 2*M*). A six-pulse optogenetic stimulation (2 Hz; pulse duration 1 ms) of the BLA- and mPFC-to-NAc projections evoked reliable action potential firing in the FSI but many fewer action potentials in the MSN (Fig. 2*N*). We then voltage-clamped the FSI at −85 mV to prevent action potential firing. When this single FSI was biophysically silenced, the same optogenetic stimulation, which only elicited EPSCs in the FSI, evoked more action potentials in the MSN (Fig. 2 *O* and *P*). Thus, compromising the FSI-mediated feedforward inhibition by inhibiting only a single connected FSI is sufficient to unleash excitatory input-induced action potential firing in its adjacent MSNs.

Taken together, these results suggest that NAcSh FSIs provide a rapid and effective feedforward inhibition of MSNs, while removing this feedforward inhibition unleashes excitatory input-induced activation of NAcSh MSNs.

Cocaine Self-Administration Does Not Affect FSI–MSN Connectivity. The above results demonstrate that an FSI-mediated feedforward circuit controls the translation of excitatory inputs to the functional output in NAcSh MSNs. Given the critical role of the NAcSh MSN output in cocaine taking and seeking (15, 16), we examined whether the FSI-mediated feedforward circuit is targeted by cocaine exposure to change NAc-based circuit and behavioral responses.

We first examined FSI-to-MSN connectivity in mice after 1 or 45 d withdrawal from cocaine self-administration (Fig. S3*A*). Drug-naïve (control) mice were age-matched with mice 1 d after cocaine withdrawal. In the pairwise recording, we measured uIPSCs in the MSN, elicited by evoked action potentials in the FSI (Fig. 3*A*). In our slice preparations, ∼50% of the recorded pairs exhibited FSI-to-MSN monosynaptic transmission (13) (Fig. S1 *C*–*E*). The uIPSC amplitude, which reflects the strength of the FSI-to-MSN connectivity (17), was not affected after 1 or 45 d withdrawal from cocaine self-administration (Fig. 3*B*). The coefficient of variation (CV) of the uIPSC amplitudes over trials, which reflects basic connectivity properties such as the number of active synapses, was also not affected after 1 or 45 d withdrawal from cocaine self-administration (Fig. 3*C*). We then used a modified multiple-probability fluctuation analysis (MPFA) (18, 19) to quantify the presynaptic release probability of FSI-to-MSN transmission. This analysis involved eliciting a train of five uIPSCs at 10 Hz such that each uIPSC within the train was elicited under a different presynaptic Ca^{2+} condition, conferring different release probabilities (Fig. 3*D*). By plotting the variances vs. means of the amplitudes of these IPSCs, a parabolic fitting can be used to derive the presynaptic release probability (Pr), number of release sites (N), and quantal size (Q) (*Materials and Methods* and Fig. 3*E*). The Pr, N, or Q of FSI-to-MSN transmission was not affected in mice after 1 or 45 d withdrawal from cocaine self-administration (Fig. 3*F* and Fig. S2 *E* and *F*). Taken together, these results suggest that the basic connectivity and transmission efficacy of FSI-to-MSN synapses are not changed by cocaine self-administration.

Highly enriched in CB1, FSI-to-MSN presynaptic terminals are regulated by endocannabinoid-CB1 signaling (12). On presynaptic terminals to MSNs, CB1 is targeted by cocaine exposure to change synaptic properties (20, 21). To examine whether FSI CB1 signaling is altered by cocaine exposure to change the FSI-to-MSN transmission and the FSI-mediated feedforward circuit, we focused on depolarization-induced suppression of inhibition (DSI), a form of CB1-mediated short-term presynaptic plasticity

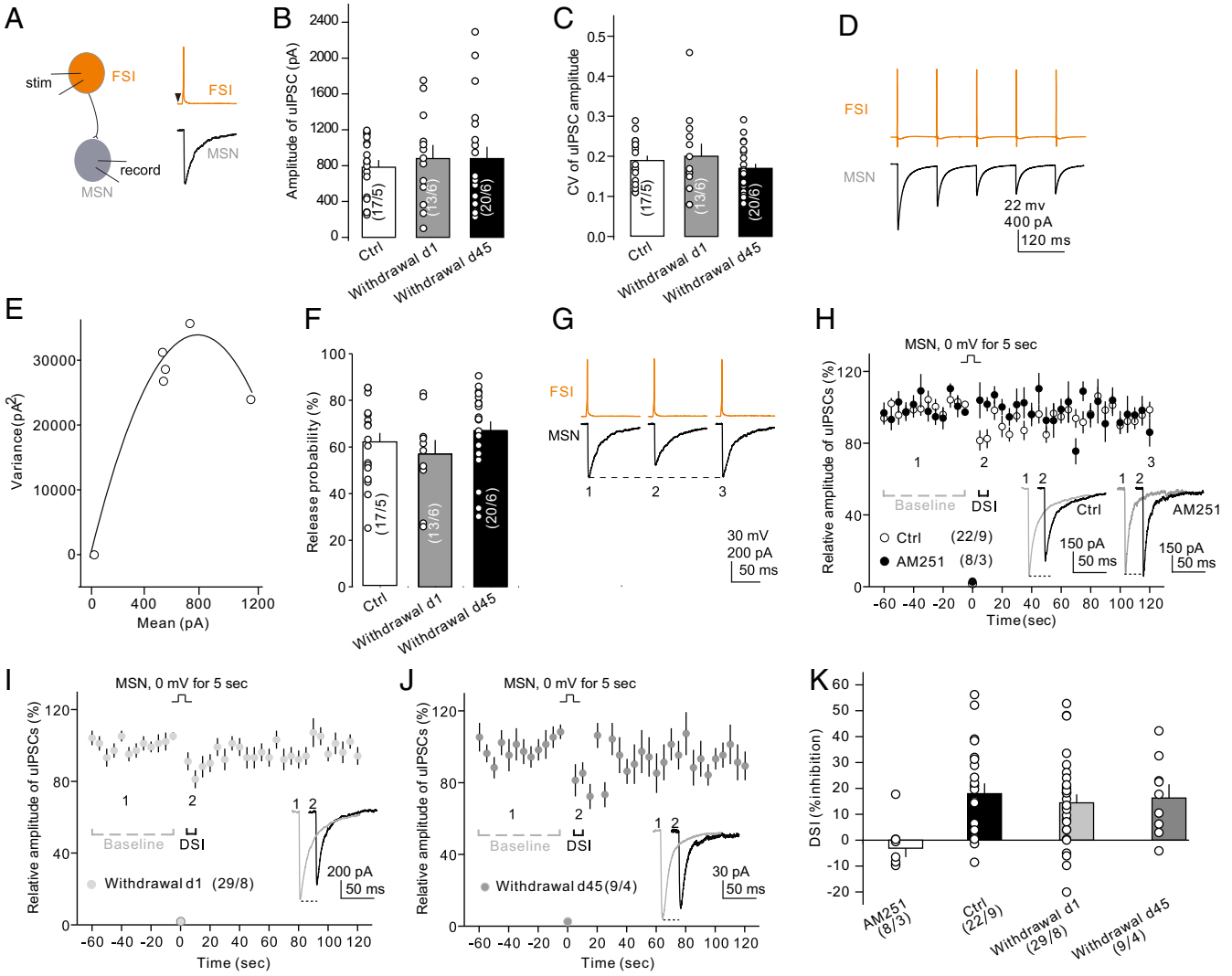

Fig. 3. Cocaine self-administration does not affect the FSI-to-MSN synaptic connectivity. (*A*) Diagram and example traces showing the pairwise recording in which uIPSCs were recorded from the MSN in response to the evoked action potential in the FSI. (*B* and *C*) Summarized results showing that neither the mean amplitudes (*B*) nor the CV of uIPSC at FSI-to-MSN synapses (*C*) were altered after 1 or 45 d withdrawal from cocaine self-administration. (*D* and *E*) Example uIPSCs (*D*) and the variance vs. mean plot of uIPSC amplitudes (*E*) at FSI-to-MSN synapses. (*F*) Summarized MPFA results showing that the Pr of FSI-to-MSN synapses was not affected 1 or 45 d after cocaine self-administration (control, 61.8 ± 4.3%, n = 17/5; withdrawal d 1, 59.7 ± 5.5%, n = 13/6; withdrawal d 45, 67.2 ± 4.0%, n = 20/6; $F_{2,47}$ = 0.81, P = 0.45, one-way ANOVA). (*G*) Example FSI-to-MSN uIPSCs before, right after, and 2 min after a 5-s depolarization of the MSN. (*H–J*) Summarized results showing that DSI of FSI-to-MSN synaptic transmission, which was prevented by AM251 (*H*), was not affected 1 d (*I*) or 45 d (*J*) after cocaine self-administration (percent inhibition by depolarization: AM251, −3.1 ± 3.5, n = 8/3; control, 18.0 ± 4.0, n = 22/9; withdrawal d1, 14.5 ± 3.3, n = 29/8; withdrawal d45, 16.3 ± 5.3, n = 9/4, $F_{2,57}$ = 0.26, P = 0.77, one-way ANOVA). (*K*) Summarized results showing that the magnitudes of FSI-to-MSN DSI were similar in mice with or without cocaine exposure (percent inhibition: AM251, −3.1 ± 3.5, n = 8/3; control, 18.0 ± 4.0, n = 22/9; withdrawal d1, 14.5 ± 3.3, n = 29/8; withdrawal d45, 16.3 ± 5.3, n = 9/4, $F_{2,57}$ = 0.259, P = 0.773, one-way ANOVA).

triggered by postsynaptic depolarization-induced endocannabinoid release (22). We performed pairwise recordings to isolate FSI-to-MSN uIPSCs (Fig. 3*A*). In slices from drug-naïve mice, a 5-s depolarization of MSNs induced DSI, an immediate and transient inhibition of FSI-to-MSN uIPSCs, which was prevented in the presence of the CB1-selective antagonist AM251 (2 μM) (Fig. 3 *G* and *H*). This FSI-to-MSN DSI was intact after 1 or 45 d of withdrawal from cocaine self-administration (Fig. 3 *I–K*).

Collectively, the above results suggest that the FSI-to-MSN segment of the feedforward circuit is not changed by cocaine exposure.

Cocaine Self-Administration Potentiates BLA-to-FSI Transmission. We next tested whether excitatory inputs to FSIs, which are the driving force of the feedforward circuit, were altered by cocaine exposure. In optogenetic-electrophysiological experiments, the intrinsic variations of ChR2 expression levels and slice preparations did not allow us to directly compare the overall BLA-to-FSI synaptic strength between mice. Instead, we performed MPFA, in which we elicited a train of seven consecutive EPSCs in each trial through optogenetic stimulation of the BLA-to-NAc projection. The Pr of BLA-to-FSI synapses was increased after 1 d as well as 45 d of withdrawal from cocaine self-administration (Fig. 4 *A–D* and Fig. S3 *B* and *C*). In contrast, the Pr of mPFC-to-FSI synapses was not altered at either of these two withdrawal time points (Fig. 4 *E–H* and Fig. S3 *D* and *E*). Note that although the Pr varied substantially among sampled synapses, suggestive of dichotomous distributions, it is statistically consistent with normal distributions (Fig. 4 *D* and *H*). Thus, the BLA-to-FSI projection is targeted by cocaine exposure to enhance FSI-mediated feedforward inhibition of NAcSh MSNs.

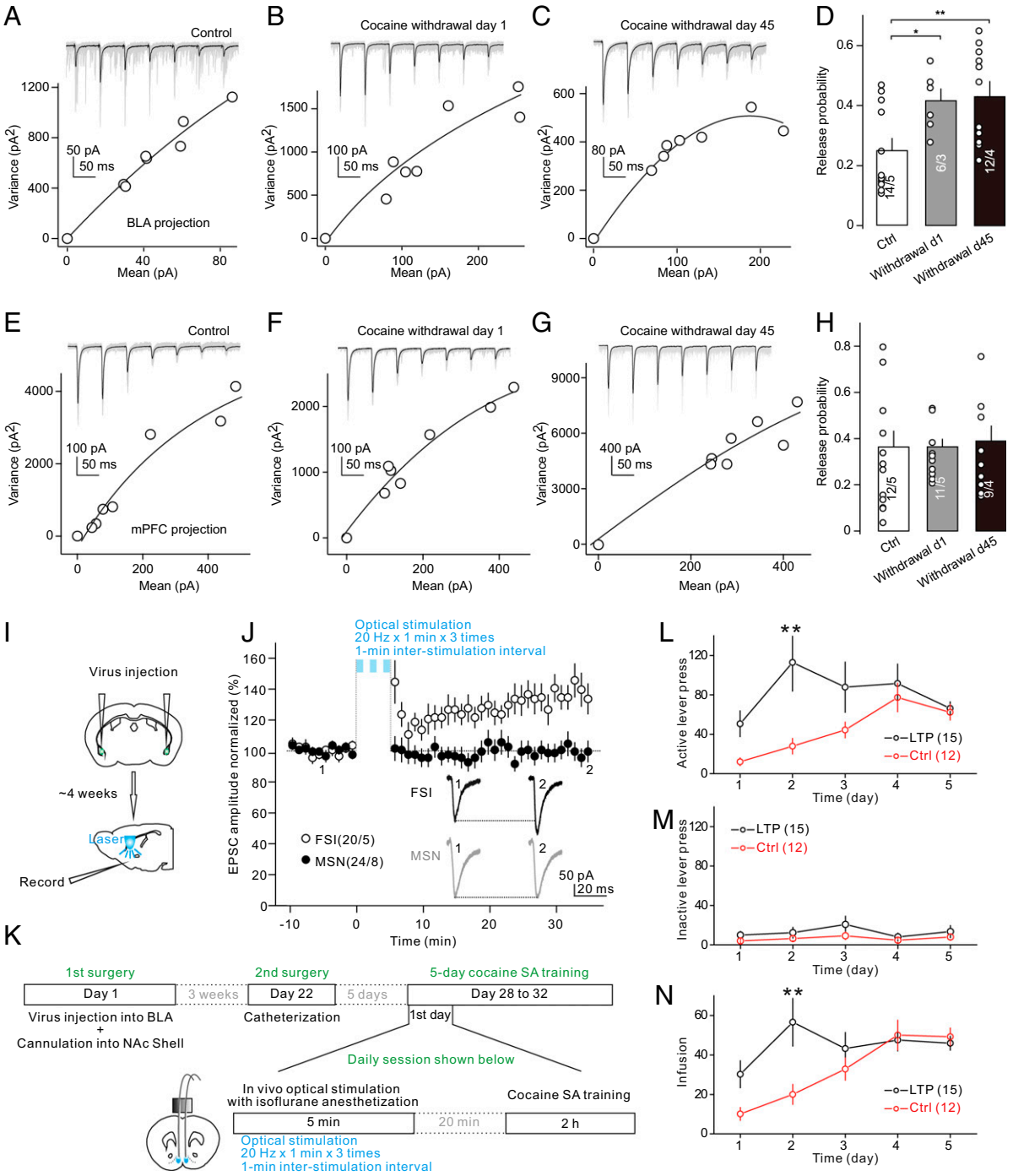

Fig. 4. The BLA-to-FSI projection in cocaine self-administration. (*A–C*) Example MPFA recordings of BLA-to-FSI synaptic transmission in control mice (*A*) and mice 1 d (*B*) or 45 d (*C*) after cocaine self-administration. (*D*) Summarized results showing that the Pr of BLA-to-FSI synapses was increased after 1 or 45 d withdrawal from cocaine self-administration (control, 0.25 ± 0.04, n = 14/5; withdrawal d 1, 0.41 ± 0.04, n = 6/3; withdrawal d 45, 0.43 ± 0.05, n = 12/4; $F_{2,30}$ = 7.72, P = 0.00, one-way ANOVA; control vs. withdrawal d 1, P = 0.03; control vs. withdrawal d 45, P = 0.00, Tukey's posttest; one-sample Kolmogorov–Smirnov test: control P = 0.18, d 1 P = 0.17, d 45 P = 0.55). (*E–G*) Example MPFA recordings of mPFC-to-FSI synaptic transmission in control mice (*E*) and mice 1 d (*F*) or 45 d (*G*) after cocaine self-administration. (*H*) Summarized results showing that the Pr of mPFC-to-FSI transmission was not affected by cocaine exposure (one-sample Kolmogorov–Smirnov test: control P = 0.90, d 1 P = 0.82, d 45 P = 0.93). (*I*) Diagrams showing the experimental setup, in which we expressed ChR2 in the BLA and recorded BLA-to-MSN or BLA-to-FSI synaptic transmission by optogenetically stimulating the BLA-to-NAc projection in the NAcSh. (*J*) Summarized results showing that the optogenetic LTP induction protocol (20 Hz × 1 min × three times, with 1-min interstimulation interval) persistently potentiated BLA-to-FSI synaptic transmission without affecting BLA-to-MSN synaptic transmission (percent of baseline 30 min after LTP: FSI, 133.4 ± 10.3, n = 20/5; MSN, 98.9 ± 6.8, n = 24/8; P = 0.006, t test). (*K*) Diagrams showing the workflow of behavioral experiments, in which mice first received intra-BLA injection of ChR2-experssing AAV and self-administration surgery and after recovery received bilateral intra-NAc optogenetic stimulations for BLA-to-FSI LTP induction before the 2-h self-administration training every day. (*L–N*) Summarized results showing that prestrengthening of BLA-to-FSI transmission expedited the acquisition of cocaine self-administration by promoting active lever press ($F_{4,100}$ = 3.1, P = 0.018, two-way ANOVA; second day, P = 0.00, Bonferroni posttest; *L*) without affecting inactive lever pressing ($F_{4,100}$ = 0.2, P = 0.91; *M*), resulting in increased cocaine infusion ($F_{4,100}$ = 5.4, P = 0.00, two-way ANOVA; second day, P = 0.00; *N*). *P < 0.05, **P < 0.01.

Contrasting to FSIs, we previously detected a persistent increase in the Pr at mPFC-to-MSN synapses but no change at BLA-to-MSN synapses after withdrawal from cocaine self-administration (23). These projection- and neuronal type-specific synaptic adaptations reflect complex mechanisms through which cocaine exposure shifts the FSI–MSN circuits and alters the functional output of NAcSh MSNs.

Potentiating BLA-to-FSI Transmission Expedites the Acquisition of Cocaine Self-Administration. To explore the behavioral correlates of FSI-mediated feedforward inhibition in the NAcSh, we optimized an optogenetic LTP protocol applied to BLA-to-FSI synaptic transmission. While this manipulation may not mechanistically create the same cocaine-induced adaptations, it does selectively enhance BLA-to-FSI transmission and thus functionally mimics the effects of cocaine self-administration. We first verified the efficacy and selectivity of this protocol by recording EPSCs in both MSNs and FSIs in NAc slices upon optogenetic stimulation of the ChR2-expressing BLA-to-NAc projection (Fig. 4*I*). The LTP protocol (20 Hz × 1 min × three times, 1 min apart) induced a persistent potentiation of EPSCs at BLA-to-FSI synapses but did not alter BLA-to-MSN synapses (Fig. 4*J*). Thus, the BLA-to-FSI transmission can be singled out for in vivo manipulation with this protocol.

The BLA-to-NAc projection is essential for the establishment of cue-conditioned operant behaviors (4, 24–26). We thus examined whether experimentally enhancing the BLA-to-FSI transmission affected the acquisition of cocaine self-administration. We bilaterally installed optical fibers into the NAcSh in mice with intra-BLA expression of ChR2. We trained the mice with daily 2-h self-administration sessions for 5 d (without overnight training; see *Materials and Methods*). Twenty minutes before the training session every day, we applied the LTP protocol to the BLA-to-NAcSh projection through preinstalled optical fibers. We then immediately placed the mice into the operant chambers for self-administration training (Fig. 4*K*). Control mice received the same AAV injection and optical fiber implantation but without the LTP protocol. Over the course of 5 d of training, control mice acquired cocaine self-administration slowly and gradually, while mice with daily BLA-to-FSI-specific LTP reached the plateau of lever pressing faster (Fig. 4*L*). Inactive lever pressing was similar between the LTP and control mice (Fig. 4*M*), suggesting that the in vivo optogenetic LTP protocol did not affect the reward discrimination or general motor responses. Consistent with the pattern of lever pressing, prepotentiation of the BLA-to-FSI transmission also expedited cocaine infusions over the acquisition phase of cocaine self-administration (Fig. 4*N*).

Conversely, we attempted to use LTD protocol to selectively reverse the cocaine-induced enhancement of BLA-to-FSI transmission, but the LTD induction protocols we tested could not achieve BLA-to-FSI specificity (Fig. S3 *F–H*).

Taken together, our current results suggest that the BLA-to-FSI and FSI-mediated feedforward circuit in the NAcSh are targeted by cocaine exposure to promote the establishment of cue-induced cocaine seeking and taking.

Discussion

Although FSI-mediated feedforward inhibition has long been recognized as a key circuit mechanism regulating the functional output of principal neurons, this mechanism remains underexplored in the NAc, a brain region critically implicated in addiction-related behaviors. Using genetically tagged mice combined with optogenetic tools, our current study characterizes the circuit properties and behavioral roles of an FSI-mediated feedforward circuit in the NAcSh. Our results suggest that widespread connections from a small population of FSIs mediate feedforward inhibition of MSNs and that this inhibitory circuit is potentiated by cocaine exposure to promote drug-motivated behaviors.

FSI-Mediated Feedforward Inhibition of NAc Output. Sharply outnumbered by principal neurons, FSIs are sporadically distributed throughout the brain, each innervating tens to hundreds of principal neurons (27). A key role of local GABAergic FSIs is to regulate the translation of excitatory inputs into excitation of principal output neurons through the FSI-imbedded feedforward circuit (27). Our results demonstrate several key features of the FSI-mediated feedforward circuit in the NAcSh.

First, BLA projection-induced activation of FSIs and the resulting IPSCs in MSNs were often sufficiently fast and strong to alter the probability and timing of the first action potential in MSNs following stimulation of the BLA-to-NAc projection (Fig. 2). Thus, in the isolated BLA-to-NAc circuit, BLA-evoked activation of NAcSh MSNs is strongly constrained by the FSI-mediated feedforward circuit. However, in behaving animals, striatal MSNs are constantly activated by excitatory inputs (28). Thus, there must also be disinhibition mechanisms, either within or outside of the BLA-to-NAc circuit, through which NAcSh MSNs circumvent the FSI-mediated feedforward inhibition. A potential mechanism is CB1-mediated inhibition of FSI-to-MSN transmission. Upon repeated activation of the BLA-to-NAc projection and glutamate release, mGluR1 on MSNs can be activated, and the resulting postsynaptic release of endocannabinoids may induce CB1-dependent inhibition of FSI-to-MSN synapses to compromise the feedforward inhibition (29). Outside of the BLA-to-NAc circuit, extracellular signals, such as monoamine systems that are selectively activated during certain behavioral responses (30), may differentially regulate the excitatory inputs to NAc FSIs vs. MSNs, resulting in an escape of MSNs from FSI-mediated inhibition. Collectively, the FSI-mediated feedforward circuit efficiently can shunt the background activation of NAc MSNs but can be circumvented in some conditions for specific outputs of NAc MSNs.

Second, MSN–FSI pairwise recordings reveal that inactivation of a single FSI is sufficient to unleash excitatory input-evoked action potential firing in adjacent NAcSh MSNs (Fig. 2). Thus, similar to striatal MSNs (11), each NAcSh MSN is likely to be innervated by a very small number of FSIs, and the output of MSNs is highly sensitive to the changes in FSIs. Furthermore, each FSI often innervates a large number of principal neurons (11). Thus, a change in FSIs can result in a large-scale change in NAcSh MSNs.

Third, FSI-to-MSN synapses provide direct inhibitory control of NAcSh MSNs, with a reversal potential of ∼−60 mV (Fig. 2). This whole-cell current-clamp measured reversal potential is consistent with the reversal potential of randomly sampled GABAergic synapses on NAcSh MSNs measured by perforated patch-clamp recording (31). Given that both FSIs and MSNs are constantly activated in vivo, FSI-to-MSN synapses may also provide a basal inhibition of MSNs in addition to the timing-contingent feedforward inhibition. It is worth noting that lateral inhibition mediated by MSN–MSN synapses does exist, and despite that the connection rate and synaptic strength are much lower than FSI–MSN synapses (13), contribute to the inhibition of MSNs.

Fourth, after cocaine self-administration, neither the basal unitary synaptic transmission nor the CB1-dependent short-term plasticity of FSI-to-MSN synapses was altered, suggesting that the FSI-to-MSN segment of the feedforward circuits is conservatively maintained. However, the excitatory inputs to NAc FSIs and MSNs are differentially and dynamically altered after cocaine exposure and withdrawal (23) (Figs. 3 and 4), indicating the plastic nature of excitatory synapses.

CB1 FSIs. In the NAc, CB1-expressing neurons are exclusively FSIs, but more than half of them do not express PV, a traditional marker for FSIs (12). Although PV-negative CB1-expressing FSIs exhibit indistinguishable biophysical and circuit properties from PV-positive FSIs, their sensitivity to CB1 signaling entails a

nonlinear inhibitory feature of the feedforward circuit. Specifically, endocannabinoids are more likely to be released from NAcSh MSNs after intensive activation (30). As such, the feedforward circuit mediated by CB1-expressing FSIs can be transiently compromised. This nonlinear feature confines the feedforward inhibition to low-intensity excitatory input-induced activation of NAcSh MSNs but spares the high-intensity input-induced activation. With this feature, the active becomes more active and the quiet becomes quieter. Such polarized patterns help secure the output of the NAcSh in response to intensive excitatory inputs from background noise. However, this CB1-mediated disinhibition is balanced by at least two other mechanisms to avoid overexcitation. Namely, CB1 is expressed at glutamatergic inputs, activation of which decreases the excitatory drive for MSN activation (30). In addition, the feedforward circuit mediated by CB1-lacking FSIs may provide persistent inhibition regardless of endocannabinoid release. Thus, multiple regulatory mechanisms operate in parallel to fine-tune the functional output of NAcSh MSNs.

Cocaine Targets the FSI-Mediated Feedforward Circuit. The BLA-to-NAc projection is essential in establishing reward-conditioned operant behaviors, including acquisition of cocaine self-administration (4, 24, 25, 32, 33). During cocaine self-administration training, BLA-to-NAc FSI transmission was enhanced, and experimentally enhancing this transmission through in vivo LTP expedited the acquisition of cocaine self-administration (Fig. 4). We propose that this cocaine-induced BLA-to-FSI potentiation is a Hebbian-like adaptation, which occurs gradually over the 5-d self-administration training, and, once achieved, promotes contingent responding. LTP pretunes the BLA-to-FSI transmission before self-administration training, resulting in increased contingent responses to cocaine during the early training days. The observation that a similar plateau of self-administration persists at d 5 in control and LTP groups (Fig. 4*N*) argues against significant damage occurring as a consequence of the LTP protocol.

While the primary rewarding effects of cocaine play an unequivocal role in the acquisition of cocaine self-administration, contingent conditioning, including the establishment and refinement of cue–cocaine association, may also be involved. Indeed, the acquisition protocol we used reveals in both control and LTP mice that, while cocaine infusions reached and maintained a plateau over training (Fig. 4*N*), lever presses tended to decrease by the end of training, suggesting an improved efficacy of contingent conditioning (Fig. 4*L*). The FSI-mediated feedforward circuit may critically contribute to this cellular-to-behavioral translation by regulating reward- or cue-induced activation vs. inhibition of NAc MSNs. Specifically, exposure to reward-conditioned cues activates a portion of BLA and NAc neurons sequentially (34, 35), while preventing activation of cocaine-sensitive NAcSh MSNs after withdrawal from cocaine self-administration attenuates cue-induced cocaine reinstatement (36). These results argue that cue-induced activation of the BLA-to-NAc projection and the resulting activation of NAc MSNs promote cue-conditioned cocaine seeking and taking. However, while some NAcSh MSNs are activated upon exposure to cocaine-associated cues, some others are inhibited, and these inhibited MSNs are also implicated in cue-induced responses (37–39). The dichotomic responses of NAc MSNs are likely implicated in two essential mechanisms, which operate cooperatively to promote cue-induced reward seeking and consumption (37, 38, 40, 41).

The NAcSh FSI-mediated feedforward circuit appears to orchestrate the dichotomic responses of MSNs upon BLA activation. Upon activation of excitatory inputs, although the averaged results show that the peak of FSI-generated IPSCs coincided with the peak of the first action potentials in NAcSh MSNs, the actual timing of the coincidence varied among MSNs within a ∼1-ms range (i.e., t3, Fig. 2*H*). In some circuit setups, FSI-generated IPSCs were slightly early, coinciding with the generation phase of the first action potential in MSNs, thus with high efficacy in suppressing the action potential generation. In some other circuit setups, FSI-generated IPSCs reached MSNs after the peak of the first, timing-contingent action potential, and thus do not affect this action potential but inhibit subsequent, noncontingent action potentials. Cocaine-induced strengthening of BLA-to-FSI transmission increases the driving force of the FSI-mediated feedforward circuit, further dichotomizing NAcSh MSNs in response to cue-induced BLA activation. Induced during cocaine self-administration training, this BLA-to-NAc-specific circuit level plasticity may help register a reinforcing value to cocaine-associated cues and contribute to the cue-elicited components during the acquisition of cocaine self-administration.

In summary, the present study characterizes an FSI-embedded feedforward circuit in the NAcSh and reveals that this circuit is targeted by cocaine to drive cue-contingent drug-taking behaviors. These results set NAc FSIs, a small neuronal population with unique biomarkers, as potential therapeutic targets to reduce drug seeking and taking.

Materials and Methods

Animals. Both male and female wild-type C57/BL mice and CB1-tdTomato knock-in mice (∼25 g; 50–90 d old) were used in all experiments. Mice were singly housed on a regular 12-h light/dark cycle (light on at 7:00 AM), with food and water available for ad libitum consumption. The animals were used in all experiments in accordance with protocols approved by the Institutional Animal Care and Use Committees at the University of Pittsburgh or Mount Sinai School of Medicine.

Drugs. Cocaine HCl (Provided by NIDA Drug Supply Program) was dissolved in 0.9% NaCl saline. Ketamine, xylazine, and acepromazine were mixed for anesthesia (purchased from a Drug Enforcement Agency-designated vendor at the University of Pittsburgh). All chemicals were purchased from Sigma-Aldrich except QX314, AM251, and Naspm, which were purchased from Tocris.

Viral Vectors. Recombinant adeno-associated vector (rAAV) 2 expressing venus tagged ChR2 H134R were pseudotyped with AAV1/2 capsid proteins. HEK293T cells were cotransfected with the plasmidspF6 (adenoviral helper plasmid), pRVI (cap and rep genes for AAV serotype 2), pH21 (cap gene for AAV serotype 1 and rep gene for serotype 2), and the rAAV plasmid, using linear polyethylenimine assisted transfection. Cultures grown in DMEM (Biochrom) with 10% substituted FBS (S0115; Biochrom) were harvested from 15- × 15-cm dishes after 48 h. rAAVs were isolated and purified. Briefly, HEK293T cells were lysed with sodium desoxycholate and repeated freeze–thaw cycles in the presence of Benzonase-Nuclease HC (Novagen). From the supernatant, rAAVs were isolated by iodixanol gradient centrifugation from the 40% and 54% interphase. rAAVs were then desalted by ultrafiltration, filtered through 0.2-μm Millex-GV filter units (Millipore), and stored at 4 °C in 500 μL PBS with 10 mM $MgCl_2$ and 25 mM KCl. The ChR2 gene was packaged with the YFP gene into a recombinant, replication-defective form of the adenovirus (AAV). We also purchased ChR2-expressing AAV2 from the University of North Carolina Virus Core. These viruses were mostly used for validation and pilot studies, and some related results were included in data analysis as well.

Viral Delivery and i.v. Surgery. Mice were anesthetized with a ketamine (50 mg/kg)–xylazine (5 mg/kg) mixture (i.p.). A 33-gauge injection needle was used to bilaterally inject 1 μL/site (0.33 μL/min) of the AAV2 solution into the BLA (in millimeters: AP, −1.10; ML, ±2.90; DV, −4.70), mPFC (AP, +1.70; ML, ±0.31; DV, −2.80), PVT (AP, −1.2; ML, 0; DV, −2.95), or vHpp (AP, −3.8; ML, ±2.80; DV, −4.75). Electrophysiological analyses were conducted 4 (withdrawal d 1) or 10 wk (withdrawal d 45) after viral injection. For mice receiving in vivo optogenetic stimulations, during the same surgical procedure stainless steel cannulas were lowered bilaterally into the NAcSh (AP, +1.50; ML, ±0.75; DV, −3.50).

For i.v. surgery, mice received the same anesthetization of viral delivery. A silastic catheter was inserted into the right auricle through the external jugular vein, and the distal end was led s.c. to the back between the scapulas. Catheters are constructed from silastic tubing (∼5 cm; inner diameter 0.020 inch, outer diameter 0.037 inch) connected to a harness (INSTECH). Catheters were flushed with sterile saline containing cefazolin (3 mg/mL) and heparin (3 UPS/mL) every 24 h during the recovery and training periods.

Self-Administration Apparatus. Experiments were conducted in operant-conditioning chambers enclosed within sound-attenuating cabinets (Med Associates). Each chamber contained an active and inactive lever, a food dispenser, the conditioned stimulus (CS) light on top of each lever and a house light. No food or water was provided in the chambers during the training sessions.

i.v. Self-Administration Training. Cocaine self-administration training began 5–14 d after surgery. In the typical procedure (all experiments except the one shown in Fig. 4 *K–N*), on d 1 mice were placed in the self-administration chamber for an overnight training session on a fixed ratio (FR) 1 reinforcement schedule. Correct lever pressing resulted in a cocaine infusion (0.75 mg/kg per infusion over 6 s) and illumination of a CS light above the lever. The CS light remained on for 20 s, whereas a house light was off for 20 s, during which active lever pressing was counted but resulted in no cocaine infusions. After the 20 s, the chamber light was turned on, and the next active lever pressing resulted in a cocaine infusion. Pressing an inactive lever had no reinforcement consequences but was recorded. Following an overnight cocaine self-administration session, mice received 6 h of cocaine self-administration daily for 8–10 d on an FR1 reinforcement schedule. For the behavioral experiments measuring the acquisition of cocaine self-administration (Fig. 4 *K–N*), the overnight training section was omitted, and mice received 2 h of daily cocaine self-administration training to extend the acquisition process.

Preparation of NAc Slices. Detailed procedures for obtaining acute NAc slices can be found in our previous publications (42, 43). Briefly, mice were decapitated following isoflurane anesthesia. Sagittal slices (250 μm) containing the NAc were prepared on a VT1200S vibratome (Leica) in 4 °C cutting solution containing (in millimolar) 135 *N*-methyl-d-glutamine, 1 KCl, 1.2 KH_2PO_4, 0.5 $CaCl_2$, 1.5 $MgCl_2$, 20 choline-HCO_3, and 11 glucose, saturated with 95% O_2/5% CO_2, pH adjusted to 7.4 with HCl. Osmolality was adjusted to 305. Slices were incubated in artificial cerebrospinal fluid (aCSF) containing (in millimolar) 119 NaCl, 2.5 KCl, 2.5 $CaCl_2$, 1.3 $MgCl_2$, 1 NaH_2PO_4, 26.2 $NaHCO_3$, and 11 glucose, with the osmolality adjusted to 280–290. aCSF was saturated with 95% O_2/5% CO_2 at 37 °C for 30 min and then allowed to recover for >30 min at 20–22 °C before experimentation.

Electrophysiological Recordings. All recordings were made in the medial NAcSh. Pairwise recordings were usually made from two adjacent neurons <50 μm apart. To record IPSCs in MSNs, pipettes were filled with a high-chloride, cesium-based internal solution [in millimolar: 15 $CsMeSO_4$, 120 CsCl, 8 NaCl, 5 TEA-Cl, 0.5 EGTA (Cs), 10 Hepes, 2 Mg-ATP, 0.3 Na_3-GTP, 5 QX-314(Br), 10 phosphocreatine, pH 7.3, 275 mM mOsm]. For other experiments, physiologically relevant internal solutions [in millimolar: 130 $KMeSO_4$, 10 KCl, 10 Hepes, 0.4 EGTA (K), 3 Mg-ATP, 0.5 Na_3-GTP, 2 $MgCl_2$, 7.5 phosphocreatine] were used unless otherwise stated. Series resistance was 9–20 MΩ, uncompensated, and monitored continuously during recording. Cells with a change in series resistance >15% were not accepted for data analysis. Synaptic currents were recorded with a MultiClamp 700B amplifier, filtered at 2.6–3 kHz, amplified five times, and then digitized at 20 kHz. Optogenetic stimulation was achieved using a blue laser with the wavelength of 473 nm (IkeCool), coupled to a 62.5-μm optic fiber. Stimulation was triggered and stimulation parameters were set by preprogrammed Clampex software (Molecular Devices). Collimated laser light was coupled to a fluorescent port of the Olympus BX51WI microscope, allowing the blue laser light to illuminate the slice through the objective. In experiments characterizing pathway-specific synaptic projections (Figs. 1 *H–M* and 4 *A–J* and Figs. S1*G* and S3 *B–H*), optogenetic stimulation duration was adjusted between 0.1 and 1.0 ms to optimize EPSC kinetics. In experiments comparing action potential firing in response to presynaptic stimulations (Fig. 2 and Fig. S2) the stimulation duration was fixed at 1.0 ms.

In Vivo Optogenetic Stimulation. For in vivo bilaterally optogenetic manipulations of the BLA-to-NAc projection, two 105-μm core optic fibers were attached to the internal cannulas through the optical neural interface (ONI). The ONI was attached with a fiber channel/physical contact (FC/PC) adaptor to a 473-nm blue laser diode (IkeCool), and laser pulses were generated through a waveform isolator (A.M.P.I.). The light intensity through the optical fiber was measured by a light sensor (S130A; Thor Labs), and adjusted to ∼10 mW. Before attaching to the ONI, the mice were anesthetized by a Small Animal Anesthesia Machine - Isoflurane (RWD Life Science Inc.). The tip of the optical fiber was placed the dorsomedial NAcSh (in millimeters: AP, +1.50; ML, ± 0.75; DV, −4.00). Thus, the potential BLA projections to both the dorso- and ventromedial NAcSh were subject to optogenetic stimulation. An optogenetic LTP protocol was administered at 20 Hz × 1 min × three times, with a 1-min interval (laser pulse duration 0.5 ms). Control mice received same anesthetization, with the same installation of optical fibers, but without laser stimulation. The mice were then placed back to their home cages until they were fully awake (∼20 min after in vivo LTP induction). The mice were then placed into the operant chambers for behavioral training and testing.

Data Acquisition and Statistics. All data were analyzed offline. Statistical results are expressed as mean ± SEM. Two-tailed *t* test or one- or two-way ANOVA was used for statistical comparisons as specified in the text. Sample size was presented as n/m, where "n" refers to the number of cells, cell pairs, or other cellular readouts, while "m" refers to the number of animals.

Both male and female mice were used. We did not detect significant difference in several electrophysiological measurements between males and females (Fig. S1 *F* and *G*), so the data were combined. In cocaine self-administration training, female mice might be more responsive to cocaine-induced behaviors, but given the relatively small sample sizes (5 males vs. 7 or 10 females in each group) we combined the data of males and females as well.

In recordings of optogenetically evoked EPSCs (Figs. 1 *H–M* and 4 *A–J* and Figs. S1*G* and S3 *B–E*), stimulation was delivered with a 15-s interpulse interval. In pairwise recording of EPSCs to FSIs vs. MSNs (Fig. 1 *H–M* and Fig. S1*G*), >30 successive sweeps were recorded and averaged. In experiments analyzing CP-AMPAR (Fig. 2 *I–L*), EPSCs were compared before and 15 min after perfusion of Naspm. In experiments accessing CB1-dependent regulations (Figs. 2 *B* and *C* and 3*H*), AM251 was bath-applied throughout the experiments. To evoke action potentials in FSI, a 1 nA × 2 ms current step was injected into the recorded neuron in all related experiments (Figs. 2 *A–E* and *M* and 3 and Fig. S1 *C–F*). In the MPFA (Figs. 3 *D–F* and 4 *A–H*), 50–120 EPSCs or IPSCs were recorded after achieving a stable baseline. In experiments accessing pathway-specific activation of FSIs (Fig. 4 *A–H*), a seven-pulse train (20 Hz) of presynaptic stimulation was used. In experiments accessing FSI-to-MSN connectivity (Fig. 3 *D–F*), a five-pulse train at 10 Hz was used to elicit action potentials in FSIs. The peak amplitude of each EPSC or IPSC was compared with its baseline and averaged to measure the mean amplitude (*I*). Variance of each EPSC/IPSC peak was calculated and plotted against their mean amplitude. We assume that presynaptic release sites operate independently and that the release probability of synapses is the same. Thus, the amplitudes of EPSCs can be expressed as

$$I = N\mathrm{Pr}Q, \quad [1]$$

where *N* is the number of release sites, Pr is the presynaptic release probability, and *Q* is the quantal size (amplitude of EPSC from release of one quantum). For a binomial model, the variance (σ^2) of EPSC amplitudes can be expressed as

$$\sigma^2 = NQ^2\mathrm{Pr}(1-\mathrm{Pr}). \quad [2]$$

Based on the two above equations, the following equation can be derived:

$$\sigma^2 = IQ - I^2/N. \quad [3]$$

This equation predicts a parabolic relationship between σ^2 and *I*. As such, the variance–mean relationship was fit with Eq. **3** to estimate *N* and *Q* in each examined cell. Pr was then calculated with Eq. **1**. If any of the theoretical assumptions do not hold true (e.g., if multivesicular release exists), the points along the σ^2–I curve would not exhibit a well-fitting parabolic relationship.

Data Exclusion. This study used a total of 325 mice, among which 15 were excluded because of the health conditions, six were excluded because they did not establish cocaine self-administration, and three were excluded because their behavioral responses were greater than threefold of SD.

ACKNOWLEDGMENTS. We thank Kevin Tang for excellent technical support. The study was supported by NIH National Institute on Drug Abuse (NIDA) Grants DA035805 and MH101147 (to Y.H.H.), DA008227 and DA014133 (to E.J.N.), DA023206 and DA034856 (to Y.D.), DA040620 (to E.J.N. and Y.D.), and German Research Foundation Grant PsyCourse SCHL592/8 and the Cluster of Excellence "Nanoscale Microscopy and Molecular Physiology of the Brain" (to O.M.S.). Cocaine was provided by the NIH NIDA Drug Supply Program.

1. Pennartz CM, Groenewegen HJ, Lopes da Silva FH (1994) The nucleus accumbens as a complex of functionally distinct neuronal ensembles: An integration of behavioural, electrophysiological and anatomical data. *Prog Neurobiol* 42:719–761.
2. Wheeler RA, Carelli RM (2009) Dissecting motivational circuitry to understand substance abuse. *Neuropharmacology* 56:149–159.
3. O'Donnell P, Grace AA (1995) Synaptic interactions among excitatory afferents to nucleus accumbens neurons: Hippocampal gating of prefrontal cortical input. *J Neurosci* 15:3622–3639.
4. Shiflett MW, Balleine BW (2010) At the limbic-motor interface: Disconnection of basolateral amygdala from nucleus accumbens core and shell reveals dissociable components of incentive motivation. *Eur J Neurosci* 32:1735–1743.
5. Bossert JM, Marchant NJ, Calu DJ, Shaham Y (2013) The reinstatement model of drug relapse: Recent neurobiological findings, emerging research topics, and translational research. *Psychopharmacology (Berl)* 229:453–476.
6. Finch DM (1996) Neurophysiology of converging synaptic inputs from the rat prefrontal cortex, amygdala, midline thalamus, and hippocampal formation onto single neurons of the caudate/putamen and nucleus accumbens. *Hippocampus* 6:495–512.
7. Lintas A, et al. (2011) Identification of a dopamine receptor-mediated opiate reward memory switch in the basolateral amygdala-nucleus accumbens circuit. *J Neurosci* 31: 11172–11183.
8. Carelli RM, Williams JG, Hollander JA (2003) Basolateral amygdala neurons encode cocaine self-administration and cocaine-associated cues. *J Neurosci* 23:8204–8211.
9. Day JJ, Carelli RM (2007) The nucleus accumbens and Pavlovian reward learning. *Neuroscientist* 13:148–159.
10. Berke JD (2011) Functional properties of striatal fast-spiking interneurons. *Front Syst Neurosci* 5:45.
11. Tepper JM, Tecuapetla F, Koós T, Ibáñez-Sandoval O (2010) Heterogeneity and diversity of striatal GABAergic interneurons. *Front Neuroanat* 4:150.
12. Winters BD, et al. (2012) Cannabinoid receptor 1-expressing neurons in the nucleus accumbens. *Proc Natl Acad Sci USA* 109:E2717–E2725.
13. Wright WJ, Schlüter OM, Dong Y (2017) A feedforward inhibitory circuit mediated by CB1-expressing fast-spiking interneurons in the nucleus accumbens. *Neuropsychopharmacology* 42:1146–1156.
14. Cull-Candy S, Kelly L, Farrant M (2006) Regulation of Ca2+-permeable AMPA receptors: Synaptic plasticity and beyond. *Curr Opin Neurobiol* 16:288–297.
15. Wolf ME (2016) Synaptic mechanisms underlying persistent cocaine craving. *Nat Rev Neurosci* 17:351–365.
16. Koob GF, Volkow ND (2016) Neurobiology of addiction: A neurocircuitry analysis. *Lancet Psychiatry* 3:760–773.
17. Kraushaar U, Jonas P (2000) Efficacy and stability of quantal GABA release at a hippocampal interneuron-principal neuron synapse. *J Neurosci* 20:5594–5607.
18. Sargent PB, Saviane C, Nielsen TA, DiGregorio DA, Silver RA (2005) Rapid vesicular release, quantal variability, and spillover contribute to the precision and reliability of transmission at a glomerular synapse. *J Neurosci* 25:8173–8187.
19. Neher E, Sakaba T (2003) Combining deconvolution and fluctuation analysis to determine quantal parameters and release rates. *J Neurosci Methods* 130:143–157.
20. Fourgeaud L, et al. (2004) A single in vivo exposure to cocaine abolishes endocannabinoid-mediated long-term depression in the nucleus accumbens. *J Neurosci* 24:6939–6945.
21. Johnson KA, Lovinger DM (2016) Presynaptic G protein-coupled receptors: Gatekeepers of addiction? *Front Cell Neurosci* 10:264.
22. Alger BE (2012) Endocannabinoids at the synapse a decade after the dies mirabilis (29 March 2001): What we still do not know. *J Physiol* 590:2203–2212.
23. Suska A, Lee BR, Huang YH, Dong Y, Schlüter OM (2013) Selective presynaptic enhancement of the prefrontal cortex to nucleus accumbens pathway by cocaine. *Proc Natl Acad Sci USA* 110:713–718.
24. Belin D, Belin-Rauscent A, Murray JE, Everitt BJ (2013) Addiction: Failure of control over maladaptive incentive habits. *Curr Opin Neurobiol* 23:564–572.
25. Di Ciano P, Everitt BJ (2004) Direct interactions between the basolateral amygdala and nucleus accumbens core underlie cocaine-seeking behavior by rats. *J Neurosci* 24: 7167–7173.
26. Lee BR, et al. (2013) Maturation of silent synapses in amygdala-accumbens projection contributes to incubation of cocaine craving. *Nat Neurosci* 16:1644–1651.
27. Hu H, Gan J, Jonas P (2014) Interneurons. Fast-spiking, parvalbumin^{+} GABAergic interneurons: From cellular design to microcircuit function. *Science* 345:1255263.
28. Mahon S, et al. (2006) Distinct patterns of striatal medium spiny neuron activity during the natural sleep-wake cycle. *J Neurosci* 26:12587–12595.
29. Younts TJ, Castillo PE (2014) Endogenous cannabinoid signaling at inhibitory interneurons. *Curr Opin Neurobiol* 26:42–50.
30. Mathur BN, Lovinger DM (2012) Endocannabinoid-dopamine interactions in striatal synaptic plasticity. *Front Pharmacol* 3:66.
31. Otaka M, et al. (2013) Exposure to cocaine regulates inhibitory synaptic transmission in the nucleus accumbens. *J Neurosci* 33:6753–6758.
32. Everitt BJ (1990) Sexual motivation: A neural and behavioural analysis of the mechanisms underlying appetitive and copulatory responses of male rats. *Neurosci Biobehav Rev* 14:217–232.
33. Meil WM, See RE (1997) Lesions of the basolateral amygdala abolish the ability of drug associated cues to reinstate responding during withdrawal from self-administered cocaine. *Behav Brain Res* 87:139–148.
34. Ambroggi F, Ishikawa A, Fields HL, Nicola SM (2008) Basolateral amygdala neurons facilitate reward-seeking behavior by exciting nucleus accumbens neurons. *Neuron* 59:648–661.
35. Tye KM, Janak PH (2007) Amygdala neurons differentially encode motivation and reinforcement. *J Neurosci* 27:3937–3945.
36. Cruz FC, et al. (2014) Role of nucleus accumbens shell neuronal ensembles in context-induced reinstatement of cocaine-seeking. *J Neurosci* 34:7437–7446.
37. Hollander JA, Carelli RM (2007) Cocaine-associated stimuli increase cocaine seeking and activate accumbens core neurons after abstinence. *J Neurosci* 27:3535–3539.
38. Ghitza UE, Fabbricatore AT, Prokopenko V, Pawlak AP, West MO (2003) Persistent cue-evoked activity of accumbens neurons after prolonged abstinence from self-administered cocaine. *J Neurosci* 23:7239–7245.
39. Guillem K, Ahmed SH, Peoples LL (2014) Escalation of cocaine intake and incubation of cocaine seeking are correlated with dissociable neuronal processes in different accumbens subregions. *Biol Psychiatry* 76:31–39.
40. Krause M, German PW, Taha SA, Fields HL (2010) A pause in nucleus accumbens neuron firing is required to initiate and maintain feeding. *J Neurosci* 30:4746–4756.
41. Larson EB, Wissman AM, Loriaux AL, Kourrich S, Self DW (2015) Optogenetic stimulation of accumbens shell or shell projections to lateral hypothalamus produce differential effects on the motivation for cocaine. *J Neurosci* 35:3537–3543.
42. Huang YH, et al. (2009) In vivo cocaine experience generates silent synapses. *Neuron* 63:40–47.
43. Ishikawa M, et al. (2009) Homeostatic synapse-driven membrane plasticity in nucleus accumbens neurons. *J Neurosci* 29:5820–5831.